

Novel strategy for fault e-diagnosis of wind energy conversion systems using wavelet analysis based on Rt-Lab and Arduino

Ahmed Cheriet¹, Abdeldjebar Hazzab^{1,2,3}, Abdelkader Bekri¹, Hicham Gouabi¹, Mohamed Habbab¹,
Miloud Rezkallah^{2,3}, Amrisha Chandra³, Hussein Ibrahim²

¹Laboratoire de recherche Commande, Analyse et Optimisation des Systèmes Électro-Énergétiques (COASEE),
Tahri Mohamed University, Bechar, Algeria

²Energy Intelligence Research and Innovation Center (CR2ie) Cégep de Sept-Îles, Sept-Îles, Québec, Canada

³Department of Electrical Engineering, École de Technologie Supérieure, Montréal, Québec, Canada

Article Info

Article history:

Received Aug 18, 2022

Revised Dec 18, 2022

Accepted Dec 29, 2022

Keywords:

Aero generators
e-Diagnosis
Hardware in the loop
Wavelet transforms
Wind turbine

ABSTRACT

The diagnosis of wind energy conversion systems (WECS) turns out to be necessary because of their relatively high cost of operation and maintenance. Wind turbines are hard-to-access structures, and they are often located in remote areas. Therefore, a remote diagnosis (e-diagnosis) is required. This paper proposes an alternative approach for the e-diagnosis of a WECS based on the discrete wavelet transform (DWT) and frequency analysis of the aero generator stator currents. To validate this approach, real-time hardware in the loop (HIL) is used to simulate in real-time the mathematical model of the induction generator on the OPAL-RT OP5600 platform to generate the stator currents and the rotor speed. The DWT is applied to the current signal, to generate the DWT signal, which has a huge number of points that are not supported for direct transmission by the Arduino Mega RobotDyn because of its limited sample time. The absolute values of the DWT peak points (MDWT) are sent as point's packages form to the diagnosis station via the ESP8266 integrated Wi-Fi board of the Arduino Mega RobotDyn to monitor the SCIG states and determine the number of broken bars.

This is an open access article under the [CC BY-SA](https://creativecommons.org/licenses/by-sa/4.0/) license.



Corresponding Author:

Ahmed Cheriet

Laboratoire de recherche Commande

Analyse et Optimisation des Systèmes Électro-Énergétiques (COASEE), Tahri Mohamed University

Street of Independence, BP 417, Bechar, Algeria

Email: cheriet.ahmed@univ-bechar.dz

1. INTRODUCTION

Wind energy conversion systems (WECS) are becoming increasingly important throughout the world, due to the exponential decreasing of fossil fuels and increasing environmental concerns such as global warming effect and pollution [1], [2]. Nowadays, many wind turbines and industrial fields use asynchronous squirrel cage motors. Since they are robust, simple to build, easy to use and require minimum low-cost maintenance. However, as robust as they are, they keep being exposed to many failures that conduct, after a certain time, partial damage or a complete stop. The presence of a fault can trigger emergency shutdowns in an industrial process. Which causes losses in production processes [3]. To avoid these undesirable situations, fault detection and diagnosis methods, that help to detect faults since their first appearance, were invented [4]–[6].

The importance of early detection of fault locations and time in electric generators has caught the researchers' attention because it prevents the spread of damage and increases generator life [7]–[11]. Wavelet transform (WT) is a technique of signal analysis based on the use of region windows of variable size. Because the wavelets have a limited duration and frequency bandwidth, the WT is localized in the frequency as well as

time domains. The signal is represented by some coefficients that make the WT a powerful tool for both fault diagnosis and condition monitoring [12], [13].

The automated control of modern wind machines requires proactive maintenance [14] because of the operating and maintenance costs and due to the remote location of wind turbines and their difficult structures, remote diagnosis (e-diagnosis) is necessary. Research in this field is still new and only a few have been mentioned, one of which is a method where data is collected by various sensors installed on each wind turbine and transmitted via wireless communication to the monitoring station [9]. Subramaniyan and Ramesh [10], the authors used GPRS/GSM communication and embedded system integration with ZigBee wireless sensor network technology for monitoring and remote control.

This work aims to develop a centralized architecture based on the use of the OPAL-RT OP5600 platform to simulate in real-time the mathematical model of the squirrel cage induction generator (SCIG) and generate stator currents and rotor speed signals. The discrete wavelet transform (DWT) is applied to the current signal and the abstract values of the DWT output signal peak points are sent out to the Arduino Mega RobotDyn to be transmitted via Wi-Fi to the diagnosis station to monitor the SCIG states.

Among the problems of the e-diagnosis, encountered in this experiment, is the limitation of the Arduino board because of the high noise in the analog input measurements and the Wi-Fi transmission frequency. Thus, in this newly developed strategy, the DWT is applied on packages of 20ms input data to reduce the number of points transmitted at a lower frequency while maintaining the precision of the information as will be detailed later. The proposed e-diagnosis strategy has been experimentally validated in real-time hardware in the loop (HIL) simulation and has shown good results in fault monitoring and surveillance.

The article is organized as follows: in the 2nd section, the model of WECS is described; the principle of DWT application is presented in the 3rd section; in the 4th section, the proposed e-diagnosis strategy of the WECS is presented and validated in the experimental simulator; the experimental results and discussions are presented in the 5th section, and the conclusion is drawn in the 6th section.

2. MODELING OF THE WIND ENERGY CONVERSION SYSTEM

The basic diagram of the WECS is presented in Figure 1. The wind turbine drives a SCIG equipped with a capacitor excitation system. The models of these elements are presented as follows.

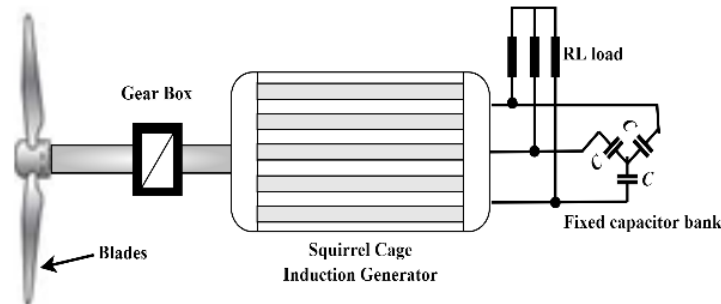


Figure 1. SCIG with a capacitor excitation system driven by a wind turbine

2.1. Model of the wind turbine

Wind turbine blades are used to convert wind kinetic Energy into electrical energy via the coupled generator. The mechanical power captured by the wind turbine is expressed by (1) [15], [16].

$$P_m = \frac{1}{2} \rho A v^3 C_p(\lambda, \beta) \quad (1)$$

Where, ρ is the air density in Kg/m^3 , A is the area swept by the turbine blades in m^2 and is equal to πR^2 , where R is the radius of the wind turbine blade, v is the wind speed in m/s and $C_p(\lambda, \beta)$ is the power coefficient. The $C_p(\lambda, \beta)$ is a non-linear function of the tip speed ratio λ and the pitch angle β , which is given by (2) and (3) [17].

$$C_p(\lambda, \beta) = 0.5176 \left(\frac{116}{\lambda_i} - 0.4\beta - 5 \right) e^{-21/\lambda_i} + 0.0068\lambda_i \quad (2)$$

$$\frac{1}{\lambda_i} = \frac{1}{\lambda + 0.08\beta} - \frac{0.035}{\beta^3 + 1} \quad (3)$$

$$\lambda = \frac{\omega_r R}{v} \quad (4)$$

Where, ω_r is the rotational speed of the blades (rad/s).

2.2. The SCIG stator equations

For more than three decades, many mathematical models-based techniques have been created [18]-[21]. The stator is given by (5).

$$v_s = R_s i_s + \frac{d\phi_s}{dt} \quad (5)$$

Were

$$v_s = [v_a v_b v_c]^T \quad (6)$$

$$i_s = [i_a i_b i_c]^T \quad (7)$$

$$R_s = \begin{bmatrix} r_s & 0 & 0 \\ 0 & r_s & 0 \\ 0 & 0 & r_s \end{bmatrix} \quad (8)$$

$$\phi_s = L_s i_s + L_{sr} i_r \quad (9)$$

$$L_s = \begin{bmatrix} L_{ls} + L_{ms} - \frac{L_{ms}}{2} & -\frac{L_{ms}}{2} \\ -\frac{L_{ms}}{2} & L_{ls} + L_{ms} - \frac{L_{ms}}{2} \\ -\frac{L_{ms}}{2} & -\frac{L_{ms}}{2} & L_{ls} + L_{ms} \end{bmatrix} \quad (10)$$

L_{ls} and L_{ms} are leakage and magnetizing inductances of the stator windings, respectively.

$$L_{ms} = \frac{\mu_0 l_r}{g} N_s^2 \left(\frac{\pi}{2} \right) \quad (11)$$

The matrix of mutual inductance stator-rotor is given by (12).

$$L_{sr} = \begin{bmatrix} L_{a1} L_{a2} \dots L_{aN_r} \\ L_{b1} L_{b2} \dots L_{bN_r} \\ L_{c1} L_{c2} \dots L_{cN_r} \end{bmatrix} \quad (12)$$

Where:

$$L_{ai} = \frac{\mu_0 l_r N_s}{g} \sin \frac{\alpha_r}{2} \cos \left(\phi_i + \frac{\alpha_r}{2} \right) \quad (13)$$

θ_i : the i^{th} bar angle, α_r : the angle between two adjacent bars.

2.3. Model of the healthy rotor

Figure 2 presents the equivalent circuit of the rotor cage, containing $k+1$ magnetically meshes. The rotor's bars are numbered from 1 to $k+1$. The two neighboring bars are joined by a segment end ring to define each mesh. In addition, as shown in Figure 2, each end ring segment and rotor bar is represented by a resistor and inductor equivalent circuit. The rotor equation can be written:

$$v_r = R_1 i_r + \frac{d\phi_r}{dt} \quad (14)$$

With:

$$\phi_r = L_{sr}^T i_s + L_r i_r \quad (15)$$

$$i_r = [v_{r1} v_{r2} \dots v_{rk} \dots v_{rN_r} v_e]^T = 0 \tag{16}$$

$$i_r = [i_{r1} i_{r2} \dots i_{rk} \dots i_{rN_r} i_e]^T \tag{17}$$

$$\phi_r = [\phi_{r1} \phi_{r2} \dots \phi_{rk} \dots \phi_{rN_r} \phi_e]^T \tag{18}$$

The rotor resistance matrix ($N_r \times N_r$):

$$R_r = \begin{bmatrix} R_o & -R_b & 0 & \dots & 0 & -R_b \\ -R_b & R_o & -R_b & \dots & \cdot & 0 \\ 0 & -R_b & R_o & \dots & \cdot & \cdot \\ \cdot & \cdot & \cdot & \dots & \cdot & \cdot \\ \cdot & \cdot & \cdot & \dots & R_o & -R_b \\ -R_b & \cdot & \cdot & \dots & -R_b & R_o \end{bmatrix} \tag{19}$$

$$R_o = 2(R_b + R_e) \tag{20}$$

$$L_o = L_{mr} + 2(L_b + L_e) \tag{21}$$

$$L_{mr} = \frac{\mu_0 l r}{g} a_r \left(1 - \frac{a_r}{2\pi}\right) \tag{22}$$

$$L_r = \begin{bmatrix} L_0 & L_{12} - L_b & L_{13} & \dots & L_{1(N_r-1)} & L_{1N_r} - L_b \\ L_{21} - L_b & L_0 & L_{23} - L_b & \dots & \cdot & L_{2N_r} \\ L_{31} & L_{32} - L_b & L_0 & \dots & \cdot & \cdot \\ \cdot & \cdot & \cdot & \dots & \cdot & \cdot \\ \cdot & \cdot & \cdot & \dots & \cdot & \cdot \\ L_{N_r,1} - L_b & \cdot & \cdot & \dots & L_{N_r(N_r-1)} - L_b & L_0 \end{bmatrix} \tag{23}$$

$$L_{ki} = -\frac{\mu_0 l r}{g} \left(\frac{a_r^2}{2\pi}\right) \tag{24}$$

The expression of the torque is given by (25).

$$\Gamma_e = \frac{1}{2} P i_s^T \frac{\partial L_{sr}(\theta_r)}{\partial \theta_r} i_r \tag{25}$$

P : rotor poles pair number, θ_r : the electric displacement angle of the rotor in radians

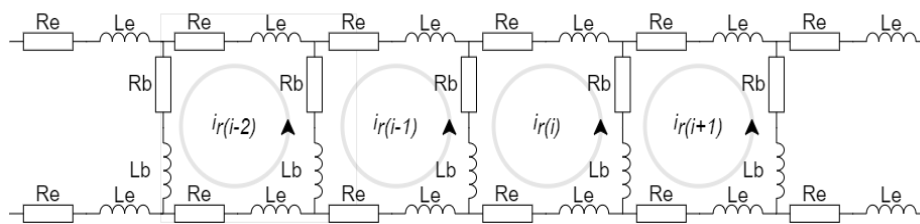


Figure 2. Equivalent circuits of a SCIG healthy rotor

2.4. Rotor modeling with rotor fault

As shown in Figure 3, the number of rotor equations is reduced according to the broken bars number, and the meshes damaged are eliminated since the i^{th} mesh will be n times larger. The mutual inductance matrix stator rotor with dimension $3 \times (N_r - n)$ becomes:

$$L_{sr} = \begin{bmatrix} L_{a1} & L_{a2} & \dots & L_{ai} & L_{a(i+(n+1))} & \dots & L_{aN_r} \\ L_{b1} & L_{b2} & \dots & L_{bi} & L_{b(i+(n+1))} & \dots & L_{bN_r} \\ L_{c1} & L_{c2} & \dots & L_{ci} & L_{c(i+(n+1))} & \dots & L_{cN_r} \end{bmatrix} \tag{26}$$

$$L_{ai} = L_m \cdot \cos\left(\theta_i + (n + 1) \frac{\alpha_r}{2}\right) \cdot \sin\left((n + 1) \frac{\alpha_r}{2}\right) \tag{27}$$

After eliminating n rows and columns of rotor matrix inductance, the new matrix of $(N_r - n) \times (N_r - n)$ dimension becomes:

$$L_r = \begin{bmatrix} L_0 & L_{12} - L_b & \dots & L_{1i} & L_{1(i+n+1)} & \dots & L_{1N_r} - L_b \\ L_{21} - L_b & L_0 & \dots & L_{2i} & L_{2(i+n+1)} & \dots & L_{2N_r} \\ \vdots & \vdots & \dots & \vdots & \vdots & \dots & \vdots \\ L_{k1} & L_{k2} & \dots & L_{0i} & L_{k(i+n+1)} & \dots & L_{kN_r} \\ L_{(k+n+1)1} & L_{(k+n+1)2} & \dots & L_{(k+n+1)i} & L_{(k+n+1)(i+n+1)} & \dots & L_{(k+n+1)N_r} \\ \vdots & \vdots & \dots & \vdots & \vdots & \dots & \vdots \\ L_{N_r1} - L_b & L_{N_r2} & \dots & L_{N_r i} & L_{N_r(i+n+1)} & \dots & L_0 \end{bmatrix} \tag{28}$$

$$L_{0i} = L_{ii} + 2(L_b + (n + 1)L_e) \tag{29}$$

$$L_{ii} = \frac{\mu_0 l r}{g} \alpha_r \left((n + 1) - (2n + 1) \frac{\alpha_r}{2\pi} \right) \tag{30}$$

$$L_{ki} = -(n + 1) \frac{\mu_0 l r}{g} \left(\frac{\alpha_r^2}{2\pi} \right) \tag{31}$$

The rotor resistance matrix with $(N_r - n) \times (N_r - n)$ dimension becomes:

$$R_r = \begin{bmatrix} R_0 & -R_b & \dots & 0 & \dots & -R_b \\ -R_b & R_0 & \dots & \cdot & \dots & 0 \\ \vdots & \vdots & \dots & \vdots & \dots & \vdots \\ \cdot & \cdot & \dots & R_{0i} & \dots & \cdot \\ \vdots & \vdots & \dots & \vdots & \dots & \vdots \\ -R_b & \cdot & \dots & \cdot & \dots & R_0 \end{bmatrix} \tag{32}$$

$$R_{0i} = 2(R_b + (n + 1)R_e) \tag{33}$$

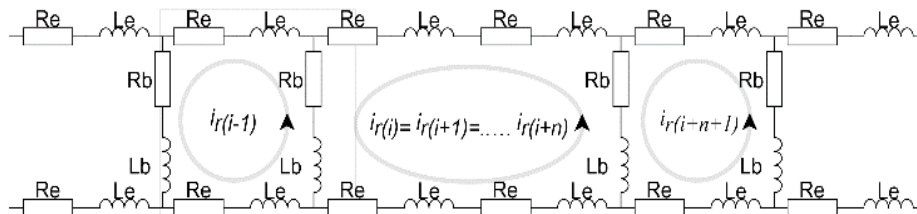


Figure 3. Equivalent circuits of a SCIG rotor with n broken bars

3. DISCRETE WAVELET TRANSFORM

The SCIG current signal faults, which appear as oscillations in the current signal spectrum, are obtained using the current signature analysis approach. The choice of the mother wavelet is completely arbitrary. As a result, selecting the mother wavelet correctly reduces errors in fault diagnosis [22], [23].

The temporal current signals are represented in the time-frequency spectrum using the symlets-DWT signal processing approach to detect the WECS SCIG broken bars number. Therefore, by selecting an initial scale to acquire the current signal characteristics, several representations of the time-frequency spectrum with different features can be observed. The augmentation of this scale allows to obtain more detailed information in the time-frequency spectrum.

The family of wavelets is obtained from a mother wavelet in Figure 4 denoted $\psi_{s,\tau}(t)$ ($\tau = s = 1$) by expansion-translation (by varying τ and s). This mother wavelet is in the form:

$$\psi_{s,\tau}(t) = \frac{1}{\sqrt{|\tau|}} \psi\left(\frac{t-s}{\tau}\right) \tag{34}$$

With s and τ are its scale and translation respectively and $s, \tau \in IR$ and $\tau \neq 0$ [24], [25].

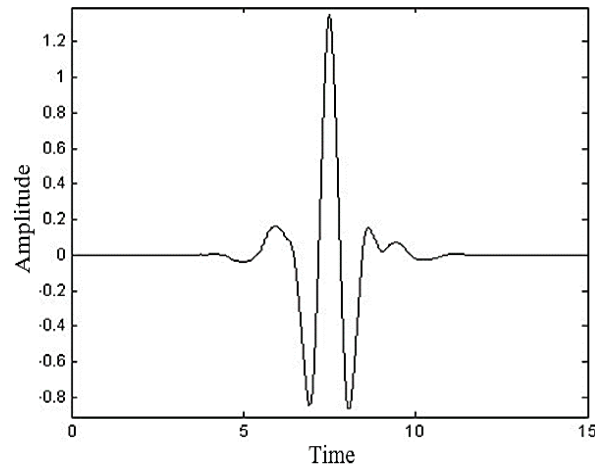


Figure 4. Symlets mother wavelet signal

4. PROPOSED FAULTS E-DIAGNOSIS STRATEGY OF WECS

The proposed strategy of WECS fault e-Diagnosis, as illustrated in Figure 5, goes through the following three main modules:

4.1. RT-LAB | OP5600-OPAL-RT

In this module, five operations are executed:

- HIL simulation of the SCIG and wind turbine assembly to generate stator currents and rotor angular speed signals (the used sample time in the HIL simulation is 0.3 ms).
- Application of the symlet DWT, order 8, levels 1 on packages of 64 points of the current signal to provide a processing signal technique for data packages of approximately 20 ms to examine and detect, in real-time, any perturbations and quick frequency variations in the current signal.
- After correlation between the current signal, obtained from de HIL simulation, and the mother wavelet, the current signal will be decomposed at different levels called detail and approximation coefficients. A comparison between the healthy currents and the failed ones (one, three, and five broken bars of SCIG) with different fault levels is performed by the display of coefficients which are transformed into the scale translation coefficients. To be able to take a decision on the fault's diagnosis, a simplification of the function DWT is proposed as (35):

$$MDWT(t_x) = |DWT(t_x)| \quad (35)$$

With t_x is the instances where $\frac{d(DWT(t))}{dt} = 0$, such as $0 < t < t_p$ with $t_p \approx 20ms$ is the package time range. The MDWT output signal is transmitted as an electrical signal between 0 and 4.5 V, via the FPGA analog output port of the OP5600-OPAL-RT.

4.2. Arduino RobotDyn

In this case, three operations are executed:

- For the e-diagnosis, an Arduino RobotDyn control board with a built-in ESP8266EX Wi-Fi module is used to send real-time data from RT-Lab to the diagnosis station in a remote wireless way.
- The electrical signal generated by RT-Lab is captured by the analog input of the Arduino and sent in 8 bits with a speed of 115200 baud to the Wi-Fi module.
- The Wi-Fi module starts sending data once it is connected to an access point.

4.3. Diagnosis station

A PC equipped with MATLAB/Simulink is connected to the same wireless access point as the Arduino and starts receiving data via TCP/IP protocol. A MATLAB/Simulink program is developed for real-time data receiving and showing the generator's health. The program implemented in the diagnosis station can identify in real-time the number of broken bars based on the MDWT variations.

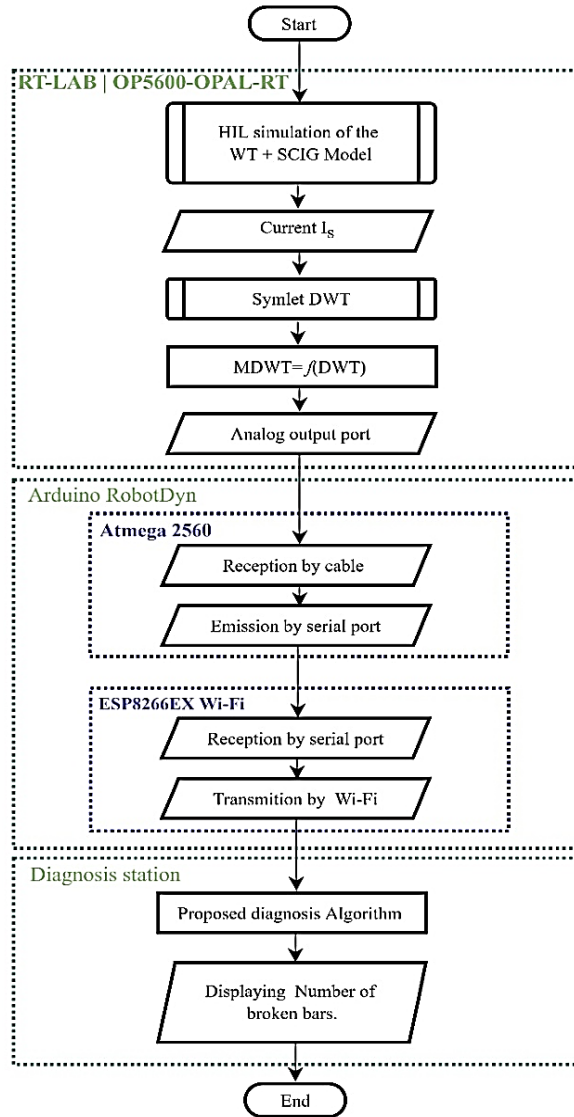


Figure 5. Proposed diagnosis flowchart

5. HIL EXPERIMENTAL RESULTS AND DISCUSSION

For the real-time HIL simulation and e-diagnosis of the isolated WECS, the experimental prototype shown in Figure 6 is used while Table 1 shows the main prototype components. As demonstrated in Figure 7, the WECS model and the current DWT are implemented in the OPAL-RT OP-5600 RT-Lab platform that generates the instantaneous MDWT signal via the analog output port. This signal is transmitted in real-time to the e-diagnosis station via Wi-Fi using an Arduino Mega data acquisition and transmission with a built-in Wi-Fi board where technical characteristics are presented in Table 2, while characteristics of the diagnosis station are presented in Table 3. The characteristics of the access point that interconnects the e-diagnosis station and Arduino are given in Table 4. The SCIG parameters used in the HIL real-time simulation for the different operating conditions are given in Table 5.

Table 1. Components of the developed experimental HIL simulation prototype

N°	Designation
1	OP5600 real-time digital simulator
2	Arduino compatible Mega R3 ATmega2560 and Wi-Fi ESP8266 with 32MB memory
3	TP-LINK Wi-Fi N 300Mbps Access Point
4	Host PC equipped with RT-LAB software
5	Power Bank
6	Oscilloscope
7	e-diagnosis station

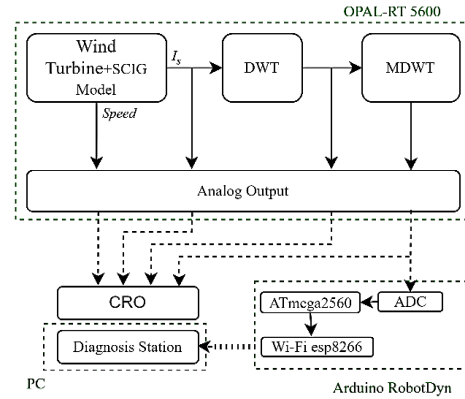
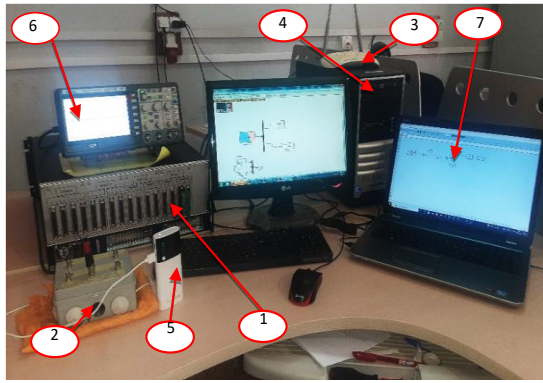


Figure 6. Photo of the experimental test bench Figure 7. Block diagram of the proposed e-diagnosis strategy

Table 2. Technical characteristics of the RobotDyn Arduino

Parameters	Description
Microcontroller	ATmega2560 (16 Mhz)+ESP8266 (Esp8266 connects to rx3/tx3 of atmega2560)
Flash memory	32Mb,
Interface	Micro-USB-TTL CH340G(converter ch340g USB connects to rx0/tx0 of atmega2560)
Pin input/output	Digital I/O Pins 70, 16 analog inputs, 14 PWM, 4 UART buses. Output current for 5 V - about 800 mA, for 3.3 V – 180 mA
Pigtail connector	Connecting an antenna on this device, you will increase your reach, right from 90 meters to 240 meters
Supply voltage	Operating voltage 5 V

Table 3. Diagnostic station characteristics

Parameters	Description
Processor	Intel(R) Core (TM) i5-3337U CPU @ 1.80 GHz
Memory	Installed 8192 MB RAM
System type	64-bit operating system, Windows 10 Pro.
MATLAB version	2018b
Hard disk	SSD (solid state drive) 500 GB
Wireless	Wi-Fi 802.11 b/g/n

Table 4. Access point characteristics

Parameters	Description
Interface	10/100M Ethernet port (RJ45)
Wi-Fi standards	IEEE 802.11n, IEEE 802.11g, IEEE 802.11b
Frequency	2.4-2.4835 GHz
Signal rate	11n: Up to 300 Mbps (dynamic), 11g: Up to 54 Mbps (dynamic), 11b: Up to 11 Mbps (dynamic)
Transmit power	<20 dBm (EIRP)
DHCP	DHCP Server

Table 5. WECS parameters

Parameters	Symbol	Values	Parameters	Symbol	Values
Rated power (kW)	P	4	Rotor bar resistance ($\mu\Omega$)	R_b	96.94
Rated voltage (V)	V	220/380	Rotor bar inductance (μH)	L_b	0.28
Rated current (A)	I	15.2/8.8	End-ring segment resistance ($\mu\Omega$)	R_e	5
Rated speed (rpm)	Ω	1465	End-ring segment inductance (μH)	L_e	0.036
Pole-pair number	p	2	Number of rotor bars	N_r	28
Supply frequency (Hz)	f_s	50	Mean radius air-gap (mm)	r	54
Power factor	$\cos\phi$	0.83	Effective air-gap (mm)	g	0.28
Rotor inertia ($kg.m^2$)	J	0.011	Length of air-gap (mm)	l	120
Friction coefficient (Nm/rad/s)	f	$8.73e-4$	Wind(m/s)	v	7
Stator phase turns in series	N_s	156	Radius of the wind turbine blade(m)	R	1.2
Stator phase resistance (Ω)	R_s	1.5	Blades pitch angle(deg)	β	8
Stator phase leakage inductance (mH)	L_{ls}	7	Air density (Kg/m^3)	ρ	1.225
Stator magnetizing inductance (H)	L_{ms}	0.55			

To verify the efficiencies of the generalized model, the control strategy, and the diagnosis procedure, three simulation cases of the isolated WECS shown in Figure 1 are validated considering that the SCIG of the WECS is subjected to one, three, or five broken bars. In the real-time simulation, the defects are introduced by removing the blocks that define the broken bars and inserting new inductances and resistances as indicated in section 2. The suggested approach was tested on a 4 kW WECS with the detailed parameters given in Table 5. The WECS real-time simulation using HIL has been implemented with a sample time of $T_s = 0.3 \text{ ms}$.

From Figure 8 or Figure 9, it is difficult to notice the change in current variations for one or three broken bars respectively, but when five bars are broken, ripples can be observed in the stator current signal shown in Figure 10. For one broken bar speed signal in Figure 11, it is hard to figure out the speed changes, compared with 3 and 5 broken bars in Figure 12 and Figure 13 respectively where the speed decreasing can be observed.

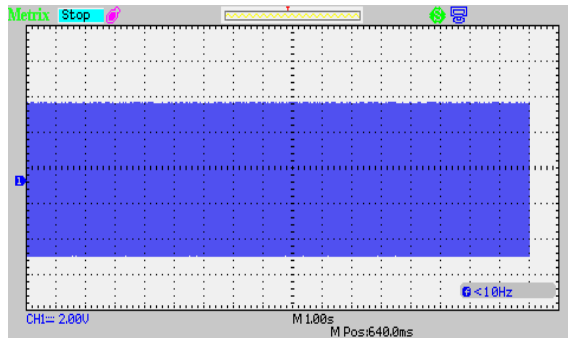


Figure 8. Stator current for 1 broken bar

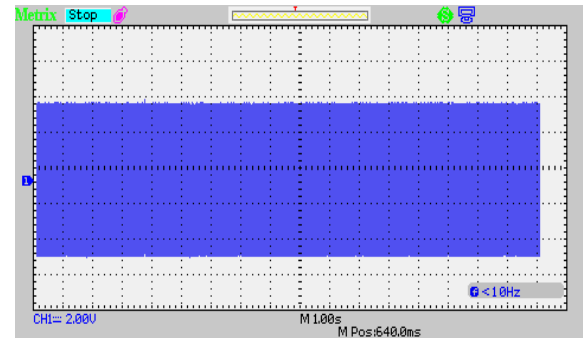


Figure 9. Stator current for 3 broken bars

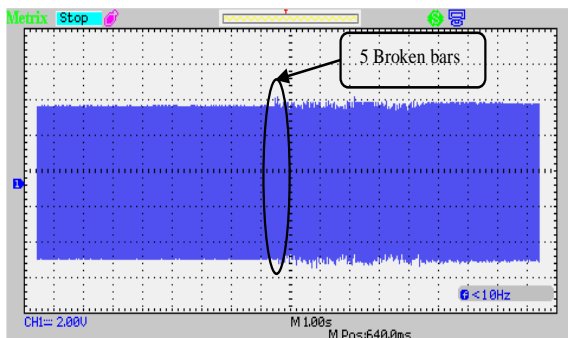


Figure 10. Stator current for 5 broken bars

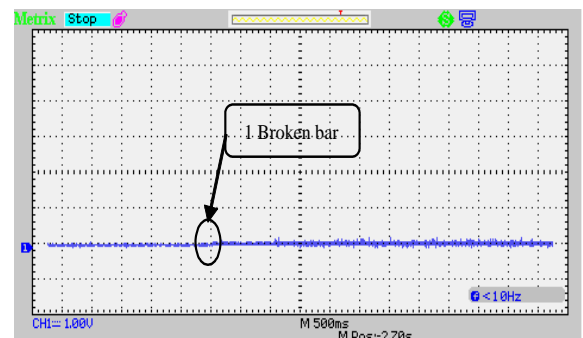


Figure 11. Rotor angular speed for 1 broken bar

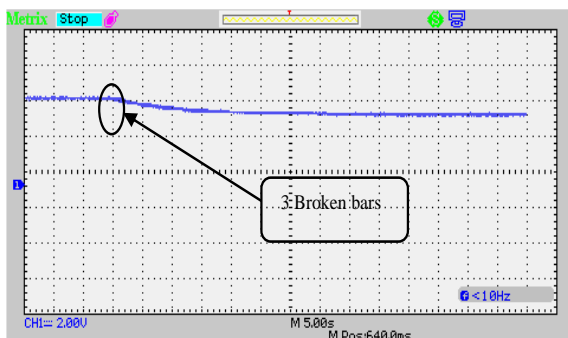


Figure 12. Rotor angular speed for 3 broken bars

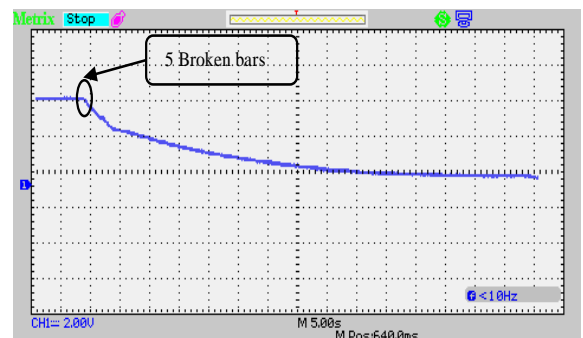


Figure. 13. Rotor angular speed for 5 broken bars

However as shown in Figure 14, Figure 15, and Figure 16, which present the DWT signal, as well as Figure 17, Figure 18, and Figure 19, which present the MDWT signal, it is easy to notice the variations of DWT and MDWT in the instances of bars breakings. Figure 20 shows the real-time MDWT signal received by the diagnosis station for 1, 3, and 5 broken bars. The signal values extracted from this figure allow us to know

the number of the broken bars, while Table 6 indicates the reference interval of MDWT values to determine the number of broken bars. This can be used to find an indirect relation between the MDWT values and the number of broken bars in the SCIG rotor.

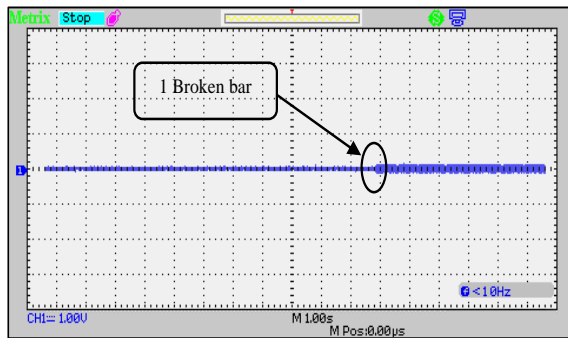


Figure 14. DWT signal for 1 broken bar

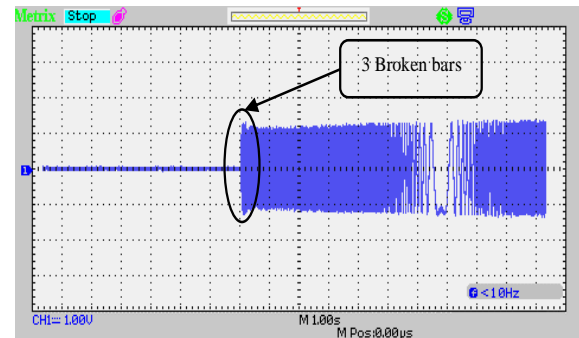


Figure 15. DWT signal for 3 broken bars

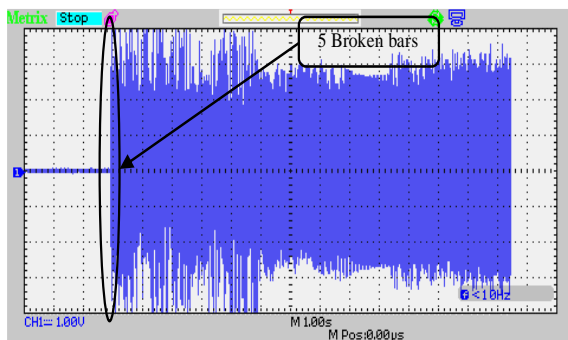


Figure 16. DWT signal for 5 broken bars

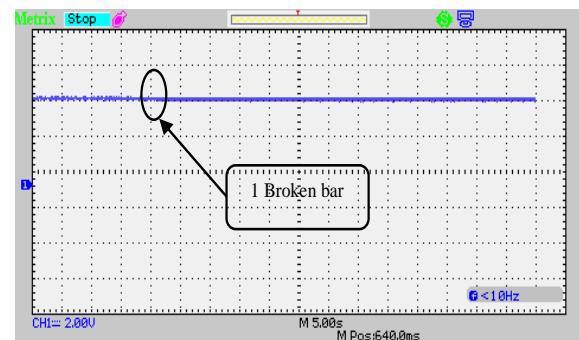


Figure 17. MDWT for 1 broken bar

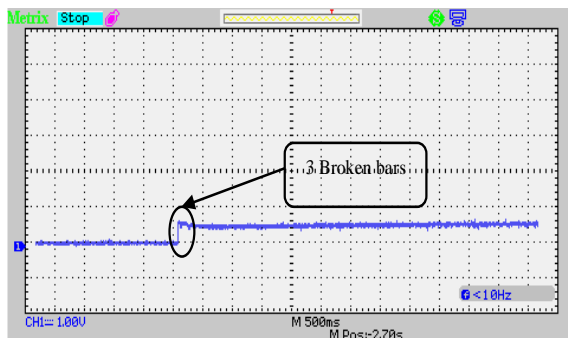


Figure 18. MDWT signal for 3 broken bars

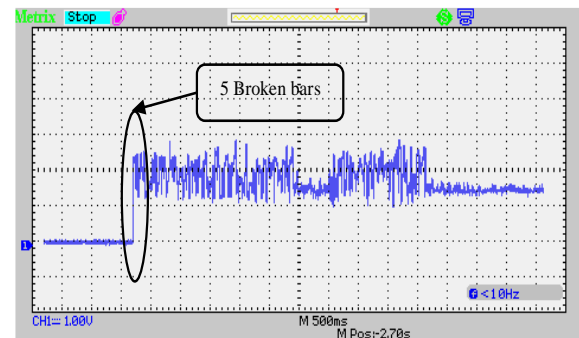


Figure 19. MDWT signal for 5 broken bars

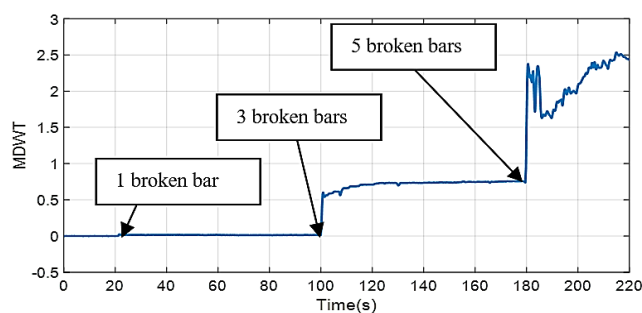


Figure 20. MDWT variation for 1, 3 and 5 broken bars

Table 6. MDWT values for different rotor broken bars

MDWT interval	Number of broken bars
$0 < \text{MDWT} \leq 6 \cdot 10^{-3}$	0
$6 \cdot 10^{-3} < \text{MDWT} \leq 0.5$	1
$0.5 < \text{MDWT} \leq 1.5$	3
$\text{MDWT} > 1.5$	5

6. CONCLUSION

The paper proposes a novel strategy for an isolated wind energy conversion system (WECS) e-diagnosis based on the discrete wavelet transform (DWT) and frequency analysis of the aero generator stator currents. This e-diagnosis strategy has been implemented in real-time for an asynchronous squirrel cage induction generator (SCIG) based on the DWT (symlet, order 8, levels 1) of the stator current signal to determine the generator's broken bars number. This proposed strategy is validated by a real-time Hardware in the loop (HIL) simulation of the mathematical model of the WECS SCIG using the RT-Lab OPAL-RT OP5600 platform. The DWT is applied to the generated current signal, it has a huge number of points which makes its transmission by Arduino Mega RobotDyn impossible because of the limited sample time of this later. The absolute values of the DWT peak points (MDWT) are sent as points packages via the Arduino integrated ESP8266 Wi-Fi module to the diagnosis station to monitor WECS states and determine the number of SCIG broken bars based on the MDWT variations. The obtained results demonstrate the applicability of this technique for the real-time analysis of different electrical variations and the instant detection of different faults.

REFERENCES

- [1] F. Poitiers, "Etude et commande de generatrices asynchrones pour l'utilisation de l'énergie eolienne," Ph.D Thesis, Ecole polytechnique de l'Université de Nantes, France, 2003.
- [2] A. Cheriet, A. Bekri, A. Hazzab, and H. Gouabi, "Expert system based on fuzzy logic: application on faults detection and diagnosis of DFIG," *International Journal of Power Electronics and Drive Systems*, vol. 9, no. 3, pp. 1081-1089, 2018, doi: 10.11591/ijpeds.v9.i3.pp1081-1089.
- [3] GWEC, "Strong outlook for wind power," *Global Wind Energy Council (GWEC)*, [Online] Available: <https://gwec.net/strong-outlook-for-wind-power-2-2/>. 2022.
- [4] M. O. Mustafa, G. Nikolakopoulos, and T. Gustafsson, "Broken bars fault diagnosis based on uncertainty bounds violation for three-phase induction motors," *International Transactions on Electrical Energy Systems*, vol. 25, no. 2, pp. 304-325, 2015, doi: 10.1002/etep.1843.
- [5] M. A. Moussa, M. Boucherma and A. Khezzer, "A detection method for induction motor bar fault using sidelobes leakage phenomenon of the sliding discrete fourier transform," *IEEE Transactions on Power Electronics*, vol. 32, no. 7, pp. 5560-5572, July 2017, doi: 10.1109/TPEL.2016.2605821.
- [6] W. T. Thomson and M. Fenger, "Current signature analysis to detect induction motor faults," *IEEE Industry Applications Magazine*, vol. 7, no. 4, pp. 26-34, 2001, doi: 10.1109/2943.930988.
- [7] K. N. Gyftakis, D. V. Spyropoulos, J. C. Kappatou and E. D. Mitronikas, "A novel approach for broken bar fault diagnosis in induction motors through torque monitoring," *IEEE Transactions on Energy Conversion*, vol. 28, no. 2, pp. 267-277, June 2013, doi: 10.1109/TEC.2013.2240683.
- [8] E. H. Bouchikhi, V. Choqueuse, M. Benbouzid, J. F. Charpentier, and G. Barakat, "A comparative study of time-frequency representations for fault detection in wind turbine," *IECON 2011 - 37th Annual Conference of the IEEE Industrial Electronics Society*, Melbourne, VIC, Australia, 2011: IEEE, pp. 3584-3589, doi: 10.1109/IECON.2011.6119891.
- [9] S. Chakkor, "E-diagnostic de processus physiques à base des méthodes de haute résolution Application: machines éoliennes," Doctorat thesis, Faculty of Sciences, University of Abdelmalek Essaâdi, Morocco, Faculté des Sciences de Tétouan, Maroc, 2015.
- [10] R. Subramaniyan and R. Ramesh, "e-diagnostic framework for electrical drive system in distributed environment," *International Journal of Applied Engineering Research*, vol. 10, no. 14, pp. 34989-34993, 2015, doi: 10.37622/IJAER/10.14.2015.34989-34993.
- [11] D. Granda, W. G. Aguilar, D. Arcos-Aviles, and D. Sotomayor, "Broken bar diagnosis for squirrel cage induction motors using frequency analysis based on MCSA and continuous wavelet transform," *Mathematical and Computational Applications*, vol. 22, no. 2, pp. 1-15, 2017, doi: 10.3390/mca22020030.
- [12] A. Ordaz-Moreno, R. de Jesus Romero-Troncoso, J. A. Vite-Frias, J. R. Rivera-Gillen and A. Garcia-Perez, "Automatic online diagnosis algorithm for broken-bar detection on induction motors based on discrete wavelet transform for FPGA implementation," *IEEE Transactions on Industrial Electronics*, vol. 55, no. 5, pp. 2193-2202, 2008, doi: 10.1109/TIE.2008.918613.
- [13] H. L. Resnikoff and R. O. J. Wells, "Wavelet Analysis: The Scalable Structure of Information," New York, NY, 2004.
- [14] S. Chakkor, M. Baghourri, and A. Hajraoui, "Wind turbine fault detection system in real time remote monitoring," *International Journal of Electrical and Computer Engineering (IJECE)*, vol. 4, no. 6, pp. 882-892, 2014, doi: 10.11591/ijece.v4i6.6479.
- [15] F. J. Lopez, G. Kenne, and F. L. Lagarrigue, "Maximum power extraction on wind turbine systems using block-backstepping with gradient dynamics control," *International Journal of Adaptive Control and Signal Processing*, vol. 31, no. 6, pp. 835-858, 2017, doi: 10.1002/acs.2733.
- [16] H. Gouabi, A. Hazzab, M. Habbab, M. Rezkallah, and A. Chandra, "Experimental implementation of a novel scheduling algorithm for adaptive and modified P&O MPPT controller using fuzzy logic for WECS," *International Journal of Adaptive Control and Signal Processing*, vol. 35, no. 9, pp. 1732-1753, 2021, doi: 10.1002/acs.3288.
- [17] M. O. Baruwa, M. Fazeli, and A. M. Egwebe, "New control paradigm for both islanded and grid-connected operation of PMSG-based wind turbine," *The Journal of Engineering*, vol. 2019, no. 18, pp. 5142-5146, 2019, doi: 10.1049/joe.2018.9359.
- [18] L. Noureddine and O. Touhami, "Diagnosis of wind energy system faults Part I: Modeling of the squirrel cage induction generator," *International Journal of Advanced Computer Science and Application (IJACSA)*, vol. 6, no. 8, pp. 46-53, 2015, doi: 10.14569/IJACSA.2015.060806.

- [19] I. Attoui and A. Omeiri, "Modeling, control and fault diagnosis of an isolated wind energy conversion system with a self-excited induction generator subject to electrical faults," *Energy conversion and management*, vol. 82, pp. 11-26, 2014, doi: 10.1016/j.enconman.2014.02.068.
- [20] T. Omar, N. Lahcene, I. Rachid, and F. Maurice, "Modeling of the induction machine for the diagnosis of rotor defects. Part I. An approach of magnetically coupled multiple circuits," *31st Annual Conference of IEEE Industrial Electronics Society, IECON, IEEE*, 2005, doi: 10.1109/IECON.2005.1569140.
- [21] R. S. Kumar, M. Manimozhi, and M. T. Enosh, "A survey of fault detection and isolation in wind turbine drives," *International Conference on Power, Energy and Control (ICPEC), IEEE*, 2013, pp. 648-652, doi: 10.1109/ICPEC.2013.6527737.
- [22] M. R. Mehrjou *et al.*, "Wavelet-based analysis of MCSA for fault detection in electrical machine," *IntechOpen edition (Wavelet Transform and Some of Its Real-World Applications)*, pp. 134, 2015.
- [23] S. Karmakar, S. Chattopadhyay, M. Mitra, and S. Sengupta, "Induction motor fault diagnosis: approach through current signature analysis (Power Systems)," *SpringerLink*, pp. 161, 2016.
- [24] M. Farge, "Wavelet transforms and their applications to turbulence," *Annual review of fluid mechanics*, vol. 24, no. 1, pp. 395-458, 1992.
- [25] C. Torrence and G. P. Compo, "A practical guide to wavelet analysis," *Bulletin of the American Meteorological society*, vol. 79, no. 1, pp. 61-78, 1998, doi: 10.1175/1520-0477(1998)079<0061:APGTWA>2.0.CO;2.

BIOGRAPHIES OF AUTHORS



Ahmed Cheriet    was born on the 16th February 1974 in Bechar, Algeria. He received the state engineer degree in computer science from the Oran University, Algeria in 1998 and the Master's degree in computer sciences from the Tahri Mohammed University, Bechar, Algeria, in 2011. He is a member of the Control Analysis and Optimization of the Electro-Energetic Systems (CAOSEE) Laboratory since 2016. His research interests cover, Power Electronics, Control Multilevel Converters, and Artificial Intelligence. He can be contacted at email: cheriet.ahmed@univ-bechar.dz.



Abdeldjebar Hazzab    received the state engineer degree in electrical engineering in 1995 from the University of Sciences and Technology of Oran (USTO), Algeria the M.Sc. degree from the Electrical Engineering Institute of the USTO in 1999, and the Ph.D. degree from the Electrical Engineering Institute of the USTO in 2006. He is currently professor of electrical engineering at University of Bechar, Bechar, Algeria, where he is Director of the Research Laboratory of Control Analysis and Optimization of the Electro-Energetic Systems, actually he is invited Professor in from École de Technologie Supérieure (ETS), Université, Montréal, Canada. His research interests include power electronics, electric drives control, and artificial intelligence and their applications. He can be contacted at email: hazzab.abdeldjebar@etsmtl.ca or abdeldjebar.hazzab@gmail.com.



Abdelkader Bekri    was born on the 4th December 1965 in Bechar. He received the state engineer degree in electrical engineering from the University of Sciences and Technology of Oran (USTO) Algeria, the M.Sc. degree from the Electrical Engineering Institute of the Tahri Mohammed University, Bechar, Algeria, and the Ph.D. degree from the Electrical Engineering Institute of the Tahri Mohammed University, Bechar, Algeria. He is currently professor of electrical engineering at University of Tahri Mohammed, Bechar, Algeria. He can be contacted at email: bekri.abdelkader@univ-bechar.dz.



Hicham Gouabi    was born on the 20th November 1992 in bechar, Algeria. He received the master degree in automation of industrial processes: automatic control from the M'Hamed Bougara University, Boumerdes, Algeria in 2016. He is a member of the Control Analysis and Optimization of the Electro-Energetic Systems (CAOSEE) Laboratory since 2016. His research interests cover, Power Electronics, Control of Multilevel Converters, Artificial Intelligence, and their applications. He can be contacted at email: gouabi.hicham@univ-bechar.dz.



Mohamed Habbab    was born in 1969 at Relizane-Algeria, received the state engineer degree in electronic engineering in 1994 from the University of Sciences and Technology of Oran (USTO), Algeria the M.Sc. degree and the Ph.D. degree in the Electrical Engineering from University Tahri Mohamed, Bechar, Algeria in 2015 and 2018 respectively. He is currently professor of electrical engineering at University Tahri Mohamed Bechar, Algeria. His research interests include power electronics, and artificial intelligence and their applications. He can be contacted at email: habbab.mohamed@univ-bechar.dz.



Miloud Rezkallah    (M'14- SM'20) received the B. Tech. degree in electrical machines and drive from the University of Science and Technology USTO, Oran, Algeria, and the M. Tech. and Ph.D. degrees in power electronics and system control from École de Technologie Supérieure (ETS), Université, Montréal, Canada., in 2010 and 2016, respectively. He is working as a senior researcher with CR2ie at Sept-Îles in Quebec and as an adjunct professor with Electrical Engineering Department at ETS. His research interests include the control and design of microgrids, renewable energy generations and applications, and energy storage systems. He can be contacted at email: miloud.rezkallah@etsmtl.ca.



Amrish Chandra    B.E. degree from the University of Roorkee, India, in 1977, the M.Tech. degree from IIT Delhi, in 1980, and the Ph.D. degree from the University of Calgary, in 1987. Before joining as an Associate Professor at the ÉTS, Montreal, in 1994, he worked as an Associate Professor at IITR. Since 1999, he has been a Full Professor of electrical engineering with ÉTS. From 2012 to 2015, he was the Director of the Multidisciplinary Graduate Program on Renewable Energy and Energy Efficiency with ÉTS. He is currently the Director of the master program in electrical engineering. The primary focus of his work is related to the advancement of new theory and control algorithms for power electronic converters for power quality improvement in distribution systems and integration of renewable energy sources. He can be contacted at email: amrish.chandra@etsmtl.ca.



Hussein Ibrahim    received a Ph.D. degree in engineering from Québec University at Chicoutimi, Canada. Since July 2009, he has research director at Cégep of Sept-Îles northern Quebec. His research interests include renewable energy sources integration, hybrid energy power system, storage energy, heat and mass transfer, fluid dynamics, and energy efficiency. He can be contacted at email: hussein.Ibrahim@itmi.ca.